A Novel SUHI Referenced Estimation Method for Multicenters Urban Agglomeration using DMSP/OLS Nighttime Light Data

Jiufeng Li, Fangfang Wang, Yingchun Fu, Biyun Guo, Yaolong Zhao, and Huafei Yu

***Abstract*—The surface urban heat island (SUHI) of urban agglomeration has always been an important topic in the studies of urban heat island, especially with the development of satellite-based land surface temperature (LST) products. However, most studies are limited to the perspective of a single city, ignoring the impact of urban agglomeration and the changes of LST at day and night on the reference LST (RLST) (e.g., rural areas). Consequently, this article proposed a novel method about SUHI intensity estimation for the multicenters (mcSUHII) of urban agglomeration in Guangdong–Hong Kong–Macao Greater Bay Area (GHMBay) using nighttime light (NTL) data (i.e., DMSP/OLS) obtained in October, 2010. The mcSUHII method considered the RLST of SUHII estimation based on multicenter structure, and was more flexible to adapt the impact of human activity intensity. The study showed that compared with other RLSTs, such as suburban and forest, mcSUHII mitigates the underestimation bias caused by ignoring the multicenter structure. Importantly, the change in SUHII for urban agglomerations is greater than for a single city. Moreover, it was illustrated that the variation of SUHII presented an obvious inverted U-shape along the gradient from the inland to the coastal cities. The highest SUHIIs in the delta cities at day and night are $\sim$7.27 $\pm$ 1.71 °C and $\sim$4.46 $\pm$ 1.42 °C, respectively. Additionally, NTL served as the dominator together with other factors that were capable of explaining more than 90% of the spatial variation in SUHII in GHMBay. Therefore, considering multicenters more in estimation of SUHII of urban agglomeration for the sustainable development.**

***Index Terms*—DMSP/OLS, Guangdong–Hong Kong–Macao Greater Bay Area (GHMBay), multicenters, surface urban heat island intensity (SUHII), urban agglomeration.**

Manuscript received November 18, 2019; revised February 18, 2020; accepted March 1, 2020. Date of publication April 2, 2020; date of current version April 21, 2020. This work was supported in part by the National Natural Science Foundation of China under Grant 41101152, in part by the Science and Technology Program of Guangdong Province, China, under Grant 2018B020207002, in part by the Open Research Fund of State Key Laboratory of Information Engineering in Surveying, Mapping and Remote Sensing, Wuhan University, China, under Grant 18T05, and in part by the Innovation Project of Graduate School of South China Normal University under Grant 2017LKXM028. (*Corresponding author: Yingchun Fu.*)

Jiufeng Li was with the School of Geography, South China Normal University, Guangzhou 510631, China, and now he is with the International Institute for Earth System Science, Nanjing University, Nanjing 210023, China. (e-mail: jiufengli@smail.nju.edu.cn).

Fangfang Wang is with the Institute of Tibetan Plateau Research, Chinese Academy of Sciences, Beijing 100101, China. (e-mail: wangfangfang19@mails.ucas.a c.cn).

Yingchun Fu, Biyun Guo, and Yaolong Zhao are with the School of Geography, South China Normal University, Guangzhou 510631, China, and also with the Guangdong Provincial Center for Smart Land Research, Guangzhou 510631, China. (e-mail: fuyc@m.scnu.edu.cn; guobiyun@m.scnu.edu.cn; zhaoyaolong@m.scnu.edu.cn).

Huafei Yu is with the School of Resource and Environmental Sciences, Wuhan University, Wuhan 430072, China. (e-mail: huafeiyu@whu.edu.cn).

Digital Object Identifier 10.1109/JSTARS.2020.2981285

I. Introduction

THE urban heat island (UHI) effect is a significant microclimate effect, which refers to a phenomenon where the temperature of a city is higher than that of the surrounding area [1], [2]. UHI has a significant impact on human health and living environment and is often focused on the canopy-layer UHI and surface UHI (SUHI) [3]–[5]. With the progress of remote sensing technology but the deficiency of meteorological stations to monitor the temperature on the continuous surface [1], [6], the satellite era of SUHI studies began in 1972 and then obtained wide application [7].

To measure the SUHI intensity (SUHII), three methods were summarized [8]. The first is that SUHI is replaced by land surface temperature (LST) [9], which mainly emphasizes the spatiotemporal variation of SUHI but ignores its intensity [8]. Second, statistical models are very efficient in describing the spatial temperature on a continuous surface, such as Gaussian surface and kernel convolution model [10], [11], while they are easily affected by climate and clouds [8]. These problems of the aforementioned methods are avoided in the third method, which refers to LST difference between the urban and surrounding reference areas and had been widely used in most studies [3], [12], [13].

To date, high-density impervious surface area (ISA) usually refers to urban areas according to its high correlation with LST [14], whereas the underlying surface that is relatively less affected by human activities, such as low-density ISA [15], water body [16], [17], cropland [18], [19], and forest [20], had been taken as the reference LST (RLST) for a single city. Compared with a single city, the urban agglomeration is a specific core area, which concentrates on a megacity generally and consists of three major cities at least [21], [22]. However, the RLST has been challenged in the following three aspects as a result of the development of urban agglomeration.

First, with the increasing growth of urban agglomeration, the thermal environment was substantially altered in a continuous area due to a decreasing or disappearing distance between city clusters [23], [24]. The development of urban agglomeration can not only increase the connectivity of ISA, but also affect the heat

exchange of ecological land, such as vegetation and water [25]. Moreover, some studies have analyzed the phenomenon that the expansion in the joint site of neighboring cities has led to its rise in LST [20], which indicates that the impact of human activities on RLST was increasing.

Second, the development of urban agglomeration erodes the surrounding forest and cropland, thereby limiting to the choice of RLST. To address this problem, the spatial variation of RLST was proposed. Moreover, researchers believed that the correlation of SUHII estimations using the different properties of RLST was weak, which caused bias to quantify SUHII in the same area [12], hence the variations of RLST should be taken into account.

Third, the variation of LST during the day and night affects the reliability of RLST. Due to the difference of solar radiation and the heterogeneity of the surface, the law of LST in the daytime is significantly different from that of the night [26]–[28]. Although previous studies related to single city have recognized that the stability of LST in rural areas is greater than urban areas [8], [9], it still ignores the diurnal variation of LST. Therefore, it is vitally important to enhance the stability of RLST by adding the changes of LST during the day and night.

The aforementioned studies showed that there were obvious differences of RLST between urban agglomeration and a single city. Therefore, to analyze the RLST and then catch the SUHII dynamics in urban agglomeration, two steps are taken. The first step is to identify the urban areas and RLST on a larger scale, such as urban agglomeration. Some methods are used for specific research, such as a buffer zone outside the pixels of the city [3], [13], classification threshold [29], Shannon entropy [30], and wavelet transform methods [31]. However, these methods mainly limited to a single-city research, which were not necessarily to be conducive to urban agglomeration. The second step is to evaluate the rationality of RLST. Ignoring the influence of urban agglomeration when selecting RLST will lead to the estimation bias of SUHII [20], or even the opposite result [24].

However, it is still unclear what method about identification of RLST and estimation of SUHII in urban agglomeration as the above stated, mainly because of the particularity of urban agglomeration. As is known to us, human activity footprints have changed the spatial pattern of natural surface energy balance through land use changes, industry, transportation, human metabolism, and other ways [32]–[36]. Therefore, it is necessary to use new methods and data to define RLST for the SUHII study in the urban agglomeration. Comparison with spectral images, nighttime light remote sensing data, as a new kind of data for detecting human activities in urban agglomeration, have two advantages. First, DMSP/OLS data can make the SUHII measurement fast, convenient, and feasible to overcome the data discontinuity in the administrative boundaries at large-scale and long time series (e.g., 1992–2012 for DMSP/OLS data and 2011 to now for NPP VIIRS data) [37]–[39]. Second, the utilization of medium-resolution DMSP/OLS (1 km) and NPP VIIRS (880 m) imagery had been proven to be able to detect the center of the urban population and the condition of society and economy [40], [41]. Herein, it can be used to reveal the SUHII gradient corresponding with the obvious thermal environment variation.

In view of the fact that Guangdong–Hong Kong–Macao Greater Bay Area (GHMBay) has become the world's largest morphologically contiguous urban agglomeration [42], in which constructed a significant three-tier spatial structure of "core-semi-marginal" [43]. This study proposed a new SUHII estimation method for urban agglomeration of GHMBay using DMSP/OLS data from the perspective of multicenters. The specific objectives of this study are as follows:

1) to build a method of extracting multicenters based on NTL;
2) to identify RLST considering the changes in LST during the day and night; and
3) to estimate the SUHII of GHMBay using mcSUHII and compare it with other methods using different RLSTs.

II. Study Area and Datasets

A. Study Area

The GHMBay, an important space carrier for China to build a world-class urban agglomeration and participate in global competition, refers to the urban agglomeration formed by nine cities in the Guangdong Province, including Guangzhou, Foshan, Zhaoqing, Shenzhen, Dongguan, Huizhou, Zhuhai, Zhongshan, Jiangmen, and two special administrative regions of Hong Kong and Macao. The land area is about 56 000 km^2, and the total length of the mainland and island coastline is 3201 km. It is a typical urban agglomeration scattered in the islands and coastal region with dense human footprints. Stretching across the Tropic of Cancer, most of cities belong to a subtropical, marine monsoon climate with an annual average temperature of 21.4–21.9 °C. The annual precipitation is 1612–1909 mm, and concentrates from April to September. Most of urban areas are of the sunny and stable climate in October when is of benefit to explore the spatial SUHI pattern across the GHMBay.

B. DMSP/OLS Nighttime Light Data

The DMSP/OLS (Version4) nonradiation-calibrated nighttime light image datasets were published by the National Geophysical Data Center under the National Oceanic and Atmospheric Administration (https://ngdc.noaa.gov/eog/DMSP/downloadV4composites.html). Each DMSP/OLS (Version4) after nonradiation calibration includes three annual average images: cloudless observation frequency images, average NTL images, and stable NTL images. The reference coordinate system of the image is WGS-84 with resolution of 30 arc seconds (approximately 1 km near the equator and approximately 0.8 km at 40° north latitude). This article extracted the NTL data of an urban–rural spatial distribution from a DMSP/OLS F18 stable NTL image of the study area obtained in October 2010. As the DMSP/OLS image grid decreases with increasing latitude [44], to correct the effects of image grid distortion and calculate the area of bright-value pixels in the image easily, the image projection was converted to the Lambert equivalent-area projection and the imagery resampled to 1 km^2. The correction of the DMSP/OLS data used the method of mutual correction and saturation correction for China [45], and the formula is shown as

$$DN_{cal} = 0.3427 * DN^{1.2188} \quad (1)$$

TABLE I
DRIVING FACTORS OF SURFACE URBAN HEAT ISLANDS

Environment factors		Data source	Links
Land cover	Artificial surfaces density (ASD) Ecological land density (ESD)	GlobalLand30	http://www.globallandcover.com
Terrain factors	Digital Elevation model (DEM),slope, surfaces roughness (SR)	GMTED	https://topotools.cr.usgs.gov/gmted_viewer
Meteorological factor	Monthly average wind speed (m/s)	Meteorology monitor stations	http://data.cma.cn/data/detail/dataCode/A.0029.0004.html

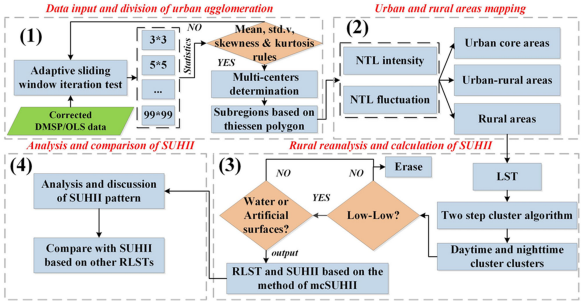

Fig. 1. Research framework.

where *DN* represents the value of pixels in the image to be corrected in 2010 and DN_{cal} represents the corrected pixel value of *DN* in 2010.

C. MODIS and Other Auxiliary Data

The MODIS series data were used for the surface temperature estimation of the Aqua satellite of the transit study area at 13:30 and 22:30 in October 2010 when the stable weather was available across the bay area. The LST/emissivity daily L3 global 1 km MYD11A1 (https://modis.gsfc.nasa.gov/data/dataprod/mod11.php) MRT (MODIS reprojection tool) was used to splice, cut, and transfer the UTM projection of daily MYD11A1 products. Other auxiliary data were combined to analyze the driving factors in the study (see Table I).

III. METHODOLOGY

The research framework of this article includes following four aspects (see Fig. 1).

1) Multicenters and subregions were extracted by the characteristics of NTL intensity and the principle of Thiessen polygon.
2) Urban and rural areas were identified by NTL intensity and its fluctuation.
3) The RLST in the rural areas was determined by considering LST changes during the day and night.
4) Comparison between the SUHII estimation and other two RLST estimation methods.

A. Multicenters and Subregions Exaction Approach Using NTL Intensity

Previous study of RLST in a single city ignored the impact of the overall development of urban agglomeration. As explained in Section I, nighttime light remote sensing data have the capability to reflect human activities, urban economy, and land use within urban agglomeration without being restricted by administrative regions. Herein, NTL can reflect the changes in human activities on the surface with the internal subregions mapping way.

According to the positive relation of NTL intensity with the urban center [37], [38], a higher NTL intensity is clustered, and a more significant center is likely to be. Based on the aforementioned theory, first, this article determined the multicenters of the urban agglomeration, thereby dividing the subregions with the help of the distance of the multicenters. This method can be achieved through the following two steps.

Step 1: The mountain vertex extraction method based on DEM was used for reference to extract multicenters in urban agglomeration [46]. First, the study area was divided into multiple windows began with 3×3 and a maximum NTL value was calculated in each window. With the iteration test of the sliding window from 3×3 to 99×99, mean, skewness, std.v, and kurtosis of the maximum NTL values in the sliding window were calculated to measure the NTL distribution. Second, the statistical distribution of each kind of iteration for the four measures was analyzed. Herein, the corresponding maximum mean, skewness value, the minimum Std.v, and kurtosis value were obtained when the window size was 79×79, as shown in Fig. 2(e). Then, the maximum mean value in the windows was used to position the pixel as the strongest NTL intensity center.

Step 2: To divide subregions in the urban agglomeration, the scheme of Thiessen polygons based on multicenters was implemented [47], [48]. First, Delaunay triangles were established based on each center, then the common vertexes of each Delaunay triangle were identified, and finally the subregions (i.e., Thiessen polygons) were created based on the common vertexes. Therefore, Thiessen polygon ensured that there is only one center in each subregion, and the distance from the boundary on the subregion to its center (human activity intensity is replaced by NTL intensity) is equal, thus this approach is more reasonable than relying on the administrative region to estimate SUHII.

B. Extraction of Urban and Rural Areas in Each Subregion Using the Characteristic of NTL Intensity

After the subregions of the urban agglomeration were divided, urban and rural areas were identified in each subregion. Mainly, the method of using NTL to divide urban and rural areas has been recognized by previous studies. The urban core area would be covered with a relatively stable and uniform NTL intensity, and both the stability and density of NTL would decrease from the center to the outside, the lowest NTL density appears in rural

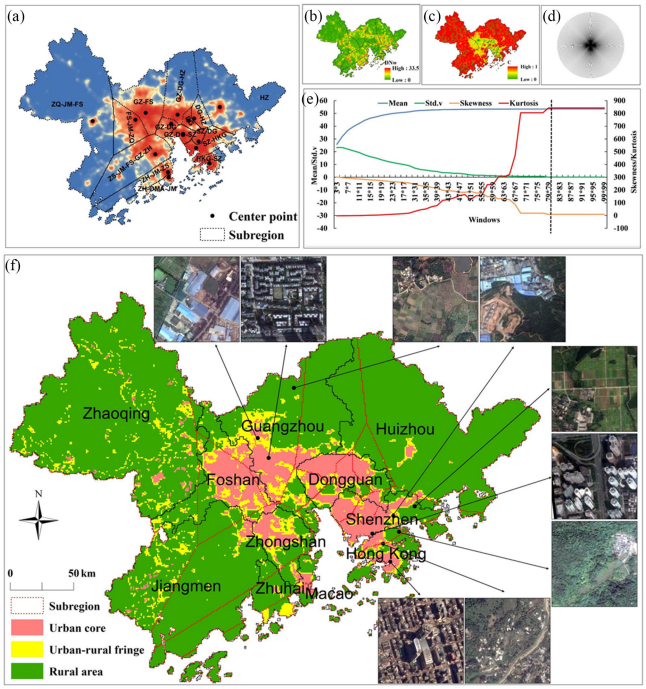

Fig. 2. Spatial patterns of urban agglomeration in 2010 in the Guangdong–Hong Kong–Macao Greater Bay Area. (a) NTL_Thiessen polygon region. (b) Calibration of nighttime light. (c) NTL fluctuation and standardization. (d) Profile line diagram. (e) Moving window size examination. (f) Google Earth image of 0.2 m.

areas [32], [49], that is, two features of NTL and NTL fluctuation can be used to characterize the three classes, including the urban core area with "high NTL, low NTL fluctuation," the urban and rural fringe with "medium NTL, high NTL fluctuation," and the rural area detected with "low NTL, low NTL fluctuation." Therefore, we used the aforementioned method to extract urban and rural areas by NTL intensity and its fluctuation in the following three steps.

Step 1: The NTL intensity had been corrected and got (1). To obtain the characteristic combination value, the NTL fluctuation was calculated using (2)–(4) [see Fig. 2(b)] [37], [50]

$$DN_w = DN_{n\max} - DN_{n\min} \tag{2}$$

$$DN_n = \frac{DN - DN_{\min}}{DN_{\max} - DN_{\min}} \tag{3}$$

$$DN_{wn} = \frac{DN_w - DN_{w\min}}{DN_{w\max} - DN_{w\min}} \tag{4}$$

where DN_w represents the NTL brightness fluctuation, $DN_{n\max}$ and $DN_{n\min}$ represent the maximum and minimum NTL intensity value in 3×3 window, respectively, DN_n and DN_{wn} represent the normalized NTL brightness and NTL fluctuation value. $DN_{\max}$, $DN_{\min}$, $DN_{w\max}$, and $DN_{w\min}$ represent the maximum and minimum of the NTL brightness and NTL fluctuation of each Thiessen polygon, respectively.

Step 2: Based on the aforementioned strategy, the combination value [C in (5)] of the intensity and the fluctuation of the NTL was calculated in each pixel [see Fig. 2(c)], which indicates the coordination degree [51], [52], the higher it is, the closer it is indicated as the pure urban or rural areas

$$\mathrm{C} = \begin{cases} 2 \times \sqrt{\frac{DN_n \times DN_{wn}}{(DN_n + DN_{wn})^2}}, & DN_n \neq 0 \text{ or } DN_{wn} \neq 0 \\ 1, & DN_n = 0 \text{ and } DN_{wn} = 0 \end{cases} \tag{5}$$

Step 3: C intersected the profile lines in each direction to get the corresponding data in 360 directions, and the attenuation distance (D_i) was extracted to obtain breakpoints in each direction [see (6)]. Finally, the breakpoint was obtained by judging D_i according to the following specific steps.

1) C for each pixel in each Thiessen polygon was scanned by creating 360 lines at an interval of 1° with the each NTL center as the circle origin [see Fig. 2(d)].
2) The distance attenuation values were calculated in each direction and the maximum distance attenuation values were got using (6), and the pixel with the maximum distance attenuation values was the breakpoint [37].
3) By measuring the distance from the breakpoint to the NTL center in regions, the abnormal points were eliminated.
4) The curve was used to connect the breakpoint and was smoothed to get the inner and outer boundary line of the urban–rural fringe, thus the urban and rural areas were identified by excluding urban–rural fringe [see Fig. 2(f)]

$$D_i = \max\left(\frac{\left|C_{ij} - C_{i(j+1)}\right|}{\sum \frac{\left|C_{ij} - C_{i(j+1)}\right|}{N}}\right) \tag{6}$$

where D_i resents the maximum distance attenuation value on the ith line, and C_{ij} and $C_{i(j+1)}$ represent the jth and $(j+1)$th sequence eigenvalues, respectively, of the ith line.

C. Multicenters SUHII Estimation Methods

First, as stated in Sections III-A and III-B, we identified multicenters by step 1 of Section III-A, and then Thiessen polygon was used to divide subregions. Finally, urban core area, urban–rural fringe, and rural area were identified in each multicenters unit (i.e., subregion or Thiessen polygon). However, rural area as a potential RLST needs further analysis for two reasons: first, the combination of daytime and nighttime LST indicates the diurnal thermal fluctuation effect of the surface heat island and second, spatial variation of SUHII corresponding with NTL appeared along the urban gradient. Hence, the RLST need to take both spatial–temporal stability and low value into consideration. To analyze potential stable regions with the lowest day and night LST variations, the two-step clustering algorithm was used in each multicenters unit to cluster LST into four modes defined as: HH (high LST during the day and night), MH (middle LST during the day but high at night), ML (middle LST during the day but low at night), and LL (low LST during the day and night). The steps consisted of preclustering, removing outlier values, and postclustering by retrieving the pixel position of LL, the potential RLST distribution can be reasonably determined [see Fig. 3(c)]. Moreover, the impact of surroundings on the RLST, such as artificial surface and water, which can be provided by the Global Land cover dataset 30 (see Table I), must be removed.

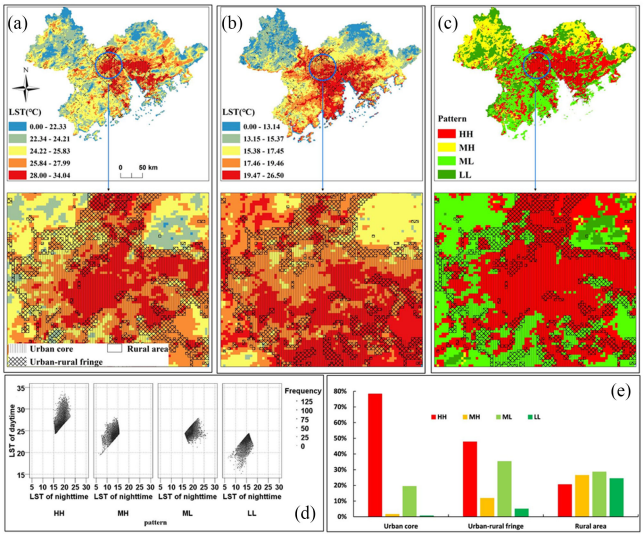

Fig. 3. Urban–rural structure of LST characteristics with (a) daytime LST, (b) nighttime LST, (c) four patterns, (d) clustering characteristics in pixels of LST during the day and night, and (e) fraction of four patterns detected with DMSP/OLS.

The SUHII (day and night) of each multicenters unit was calculated pixel by pixel according to the obtained LST of the urban area and the rural optimal RLST. The formula is shown as

$$I_{NTL} = LST_{(i,j)} - T_{NTL(i,j)} \tag{7}$$

where I_{NTL} represents the daytime or nighttime SUHII, $\mathrm{LST}_{(i,j)}$ represents the LST of the urban area at the pixel (i, j) during daytime or nighttime, $T_{NTL(i,j)}$ represents the best RLST for the SUHII calculation at the pixel (i, j).

D. Other Methods for Estimating SUHII

To compare the differences between mcSUHII and other methods, two methods in the previous studies were also used to calculate the SUHII with reference to suburban/rural region [4] and forest [20] to verify its rationality. The algorithm used in [4] was implemented by the following steps (referred as method 1).

Step 1: A continuous urban area with an artificial land surface density more than 50% was searched by means of sliding window analysis.

Step 2: All nonurban pixels surrounding the urban area were regarded as potential suburban, in which the suburban pixels were equal to the number of pixels of the urban area, and the nonurban pixels, such as artificial land surface and water, need to be excluded to avoid LST fluctuations.

Step 3: The SUHII of the urban area was calculated pixel by pixel

$$I_{SUB} = LST_{(i,j)} - T_{SUB(i,j)} \tag{8}$$

where I_{SUB} represents the daytime or nighttime SUHII, $\mathrm{LST}_{(i,j)}$ represents the LST of the urban area during daytime or nighttime, $T_{SUB(i,j)}$ represents the suburban temperature reference calculated by SUHII, and i, j represents the pixel position.

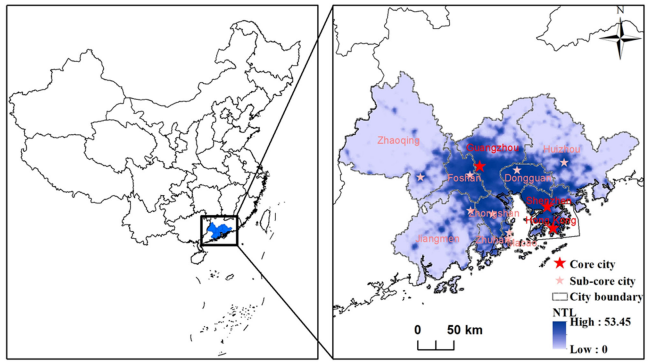

Fig. 4. Planning city centers of GHMBay.

In addition, the examination in the study of Zhou *et al.* [20] was implemented by the following steps (referred as method 2).

Step 1: This step was the same as the step 1 of method 1.

Step 2: Dense forest cover (approximately 100%) was determined as a forest reference area by pixel value search.

Step 3: The SUHII of the urban area was calculated pixel by pixel

$$I_{FOR} = LST_{(i,j)} - T_{FOR(i,j)} \tag{9}$$

where I_{FOR} represents the daytime or nighttime SUHII, $\mathrm{LST}_{(i,j)}$ represents the LST of the urban area during daytime or nighttime, $T_{FOR(i,j)}$ represents the forest temperature reference calculated by SUHII, and i, j represents the pixel position.

IV. Result

A. Urban Agglomeration Mapping

A total of 15 NTL subregions (i.e., Thiessen polygon) mapping for the spatial structure of cities in GHMBay were extracted by using the mcSHUII method. These subregions were mainly located in the dense urban areas with high-density NTLs, such as Shenzhen, Guangzhou, and Dongguan. The optimal window size for analyzing the central point was determined to be 79 × 79 after conducting the iterative test beginning from 3 × 3 to 99 × 99 [see Fig. 2(b)–(e)]. By visualization, most NTL centers seemed to be consistent with the planning centers shown in Fig. 4. Moreover, the rarer the human activity footprints were, the sparser the central points were, and the larger the region was likely to be. Therefore, a series of subregions for NTL centers were divided, including Guangzhou–Foshan, Guangzhou–Dongguan, Guangzhou–Dongguan–Huizhou, Guangzhou–Dongguan–Shenzhen, Dongguan, Dongguan–Shenzhen, Dongguan–Huizhou, Shenzhen–Hong Kong, Zhuhai–Macao–Jiangmen, and Zhuhai–Jiangmen–Zhongshan

Fig. 2(f) shows the spatial pattern of the urban core areas, urban–rural fringe, and rural areas in each subregion based on DMSP/OLS imagery. NTL centers were mostly distributed in the adjacent regions of Guangzhou, Foshan, Shenzhen, Hong Kong, Dongguan, Zhongshan, and the urban core areas were connected together. The urban–rural fringes were surrounded

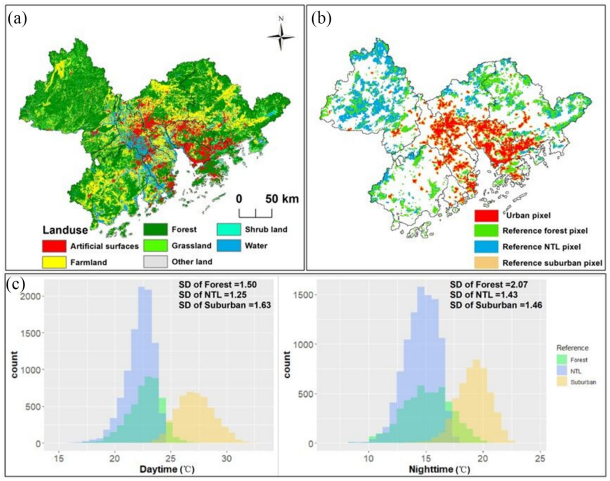

Fig. 5. (a) Global Land cover dataset of 30 m in 2010, (b) relation of urban area and reference pixels derived from NTL and suburban, forest, and (c) daytime and nighttime LST.

with the urban core, such as a ring. The urban core areas of Huizhou, Zhuhai, Macao, and Zhaoqing appeared with one center. Moreover, the urban–rural fringes were relatively dispersed but were also limited by the surrounding topography and rivers. Dense commercial services and buildings were distributed in the urban core areas, industrial land mainly located in the urban fringe areas, and large areas of farmland or mountain villages consisted of rural areas [see in Fig. 2(f)].

B. Daytime and Nighttime LST Pattern

Fig. 3 shows four clusters of daytime and nighttime LST across the urban–rural fringes, which was decreasing with the urban–rural gradient. In daytime and nighttime LST feature space, the variation range of four diurnal patterns (HH, MH, ML, and LL) indicated the similar decreasing trend, and LL was focused with both low features in Fig. 3(d). Notably, some exceptions include the low temperature that appears in the mountain or water needed to be removed. Moreover, as shown in Fig. 3(e), rural areas accounted for the largest proportion in the four clustering models in the GHMBay area. HH was focused on most of the urban core areas of 5238 km^2, which was more than twice that of the urban–rural fringe. Moreover, area proportion of LL pattern in the rural areas was far larger than the other two, which reflects the low human activity intensity there. LL clustering in rural areas could be regarded as an importantly suitable factor for RLST.

C. Spatial Pattern of SUHI

As Fig. 5 shows seven categories of land cover/use derived from Global land 30 (see Table I), and the fraction of artificial surface more than 50% was regarded as the urban land [4]. Mainly, the use of 30-m resolution pixels was beneficial to recognizing the thermal environment difference between the urban and RLST. As comparison, the three RLST pixels were displayed in Fig 3(b). Among them, the buffer zone surrounding that has the same size as urban area was defined as the suburban areas [3]. The forests 25–30 km away from urban areas that outside

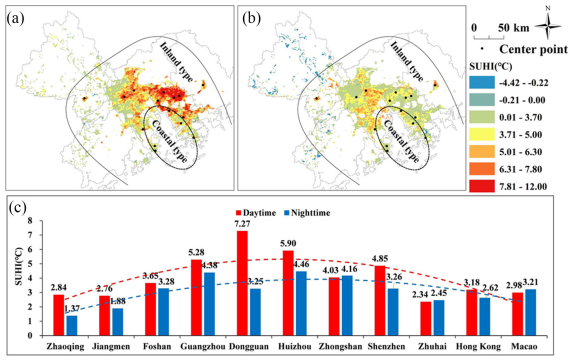

Fig. 6. Spatial distribution of SUHII in GHMBay. (a) Daytime SUHII. (b) Nighttime SUHII. (c) Mean SUHII of cities.

the UHI footprints were defined as the rural areas [20], [53]. Built-up lands, water body, and buffer areas overlapped by two or more cities were excluded. So in visualization, the suburban reference pixels were of the closest distance from urban than the other two. It was obviously mixed with some urban or urban fringe pixels. While the rural reference pixels evenly distributed across the cities as well as importantly filled the gap where lack the forest reference. For the forest vacant area, it was beneficial to take consideration of the spatial variation of driver factors of SUHI. As the statistics of daytime and nighttime LST, the rural NTL were characteristics of the lowest mean, standard error with the most pixels that mixed with the suburban one were far lower than that between the forest reference and suburb reference. Therefore, the NTL pixels appeared more stable, low LST value, and reliable spatial location to serve as reference.

Spatial pattern of daytime and nighttime SUHI are shown in Fig. 6. The high daytime SUHII concentrates in the delta cities [see Fig. 6(a)], which appeared to be strongly correlated with many SUHII centers. Daytime SUHII in these areas mainly varied within 7.9–11 °C. The high nighttime SUHII in most areas was below 6.3 °C, and mainly scattered in Guangzhou–Foshan–Zhongshan [see Fig. 6(b)]. The low-intensity SUHII (less than 3.7 °C) was dispersed surrounding possibly due to far distance from the core area of GHMBay, accompanied by some cold islands. In general, the cities can be regarded as two kinds of the inland and the coastal types according to spatial pattern of SUHII. Among them, the coastal type mainly included offshore human activity center, such as Hong Kong, Shenzhen, and Zhuhai (Macao) of which were combined as the same center due to the short distance. The rest were regarded as the inland human activity types. Fig. 6(c) shows spatial variation of the SUHII at day and night along the gradient from the inland, delta to offshore cities, which shows an inverted U-shaped curve. The distinctive daytime and nighttime SUHII difference in inland cities was significantly greater than that in coastal cities. Then, the driving factors are further discussed for the spatial pattern SUHI in the coastal areas, inland areas, and GHMBay.

V. Discussion

A. Comparison of SUHII Estimation

Previous studies used RLST at the suburban areas to reveal SUHII of a single-city research across global [3], national [31],

TABLE II
SURFACE REFERENCE LST OF TYPICAL CITIES

City	Daytime and Nighttime LST-Reference					
	Rural (the Proposed)		Forest (Zhou et al.,2018)		Suburban (Peng et al.,2018)	
Hong Kong	22.97	16.17	24.12	17.03	26.28	19.01
Shenzhen	22.86	16.18	23.76	18.17	26.53	18.76
Guangzhou	22.41	14.68	21.97	14.48	27.69	18.85
Zhaoqing	22.01	14.20	22.36	14.34	25.94	18.07

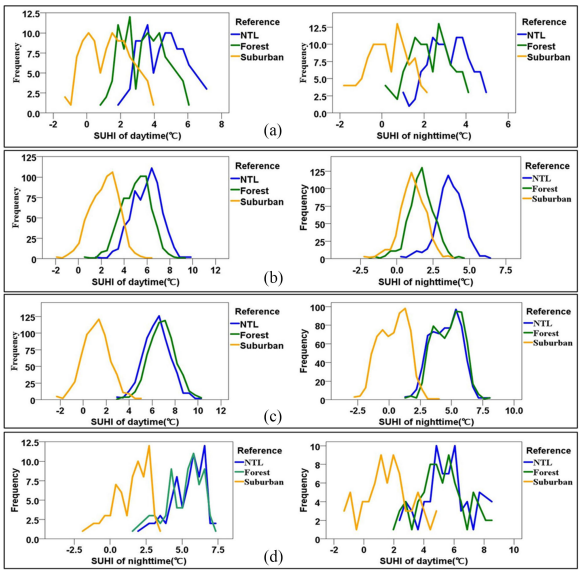

Fig. 7. Pixel statistics of SUHII in urban core areas under different RLST in the typical cities. (a) Hong Kong, (b) Shenzhen, (c) Guangzhou, and (d) Zhaoqing.

and city scales [54]–[57]. Forest reference was proposed and applied to the urban agglomeration in the Yangtze River Delta due to the relatively stable in surface coverage and temperature [20]. According to the positive correlation of human activity and SUHII, this study utilized NTL_Thessine polygon to identify multicenters and the urban–rural ranges. Moreover, the cluster of daytime and nighttime LST was beneficial to further identify low LST feature from the rural areas. To compare, three methods were also used to determine the reference LST as stated in Section IV-C. Moreover, Zhaoqing, Guangzhou, Shenzhen, and Hong Kong, which reflect the different location, different intensity of urbanization and human activity, served as the comparison. Table II illustrated the difference of the reference LST for the four cities. The mean value of LST referred to the suburb, forest and NTL_rural was the largest, the second large and the smallest one, respectively. Hence, SUHII of the three methods increased in the opposite turn (see in Figs. 3 and 7). For example, both daytime and nighttime SUHII of the proposed method were more consistent with those from the forest reference in Guangzhou and Zhaoqing, but it was higher than the other two methods in Hong Kong and Shenzhen. The two cases demonstrated the effects of different RLST on SUHII estimation both in the inland and coastal cities.

Furthermore, different with the quantitative evaluation of surface temperature products by RMSE and SIFI [58], [59], this article mainly adopted the way of SUHII comparison with existing studies. As referred the temperature observatory stations in Hong Kong and Tsak Yue Wu, the daytime SUHII in Hong Kong varied within 3–4 °C [60], which was overlaid with our study results of 2–7 °C. Moreover, the daytime SUHII in Shenzhen varied within 3–9 °C of Yuan *et al.* [61], which included our study results (4–8 °C). Correspondingly, the daytime and nighttime SUHII in autumn of Guangzhou were 4–9 °C and 2.5–7.5 °C herein, which were consistent with the results approximately 1–4 °C and 2–6 °C (see Chen *et al.* [41]), respectively. These cases showed that the SUHII calculated in this article was close to their upper limit. Therefore, it not only showed the consistency with previous studies, but also that the variation range of SUHII of multicenters in urban agglomeration was larger than that of single city. It illustrated that the NTL factors, indicated the perspective of human activities, were the dominated factors of SUHI pattern in urban agglomeration.

B. Importance of NTL for SUHII

Table III showed the enhancement effect or the nonlinear synergy of two factors as of Section IV-C stated, which was implemented in geodetector (http://www.geodetector.cn/) [62]–[65], a geographical tool widely used for linear or nonlinear detection. It is beneficial to understand the spatial variation pattern of SUHI. According to the impacts way, ASD, ESD, DEM, and slope were of the static environment factors with significant impacts. Thus, wind speed (WS) and NTL can be regarded as the dynamic factors from the climates and human behaviors impacts. NTL was the only dominant factor with a high contribution to SUHII in GHMBay, the coastal, and inland areas. Meanwhile, all two factors were of the interaction enhancement excluding the pair of NTL with WS. Moreover, the interaction between NTL with ESD performed the significant enhancement influences on the daytime SUHII in the whole bay areas. Moreover, NTL and DEM obviously dominated the variation of nighttime SUHI pattern in the whole bay areas. Therefore, compared with other factors, the analysis of spatial heterogeneity proved that NTL plays an important role in characterizing the spatial differentiation of SUHII.

C. Advantages and Limitations

The proposed method has three advantages. First, we calculated SUHII from the view of multicenters in urban agglomeration for the first time, and applied it to an example based on the GHMBay. Due to take the adaptive sliding window to extract the center and structure, the proposed method is capable to use in other areas. It is beneficial to overcome the limitation of a single

TABLE III
INFLUENCE OF DRIVING FACTOR INTERACTIONS ON THE SPATIAL PATTERN OF SUHI

	SUHI type	C=A∩B	A+B	Indication
Coastal type	Daytime	ASD∩Slope=0.60	ASD(0.44)+Slope(0.36)=0.80	III
		ASD∩SR=0.60	ASD(0.44)+SR(0.34)= 0.78	III
	Nighttime	NTL∩DEM=0.30	DEM(0.24)+NTL(0.08)=0.32	III
		DEM∩WS=0.30	DEM(0.24)+WS(0.08)=0.32	III
Inland type	Daytime	NTL∩ASD=0.60	NTL(0.50)+ASD(0.40)=0.90	III
		NTL∩ESD=0.60	NTL(0.50)+ESD(0.40)=0.90	III
	Nighttime	NTL∩DEM=0.45	NTL(0.33)+DEM(0.22)=0.55	III
		NTL∩WS=0.44	NTL(0.33)+WS(0.10)= 0.43	V
GHMBay	Daytime	NTL∩ESD=0.51	NTL(0.34)+ESD(0.38)=0.72	III
		NTL∩Slope=0.51	NTL(0.34)+Slope(0.19)=0.53	III
	Nighttime	NTL∩DEM=0.42	NTL(0.29)+DEM(0.16)=0.45	III
		NTL∩WS=0.37	NTL(0.29)+WS(0.07)= 0.36	V

Note: I. Nonlinear weakening. II. Single-factor nonlinear attenuation. III. Two-factors enhancement. IV. Independence. V. Nonlinear enhancement.

city range so as to consider the effect of the SUHI in urban agglomeration. Moreover, the daytime and nighttime LST in rural areas were separately considered, which ensure the stability of RLST. Most studies were limited to the separation of rural areas; however, in this article, clustering algorithm was used to ensure the stability of RLST in urban agglomeration, thereby reducing the estimation bias of SUHII. Third, the advantage of nighttime light data is used to break administrative restrictions. Of course, lots of data, such as the dataset of MODIS MCD12Q1, also have this advantage. Nighttime light data are suitable for the estimation of SUHII on a large scale, such as urban agglomeration because of the strong association with human activities. Especially, with the production of high-resolution nighttime light data, such as LJ (130 m) [66], [67], it is beneficial to the estimation of SUHII in small scale of multicenters in the future.

However, a few issues need to be examined further. First, this article provided a method of using Thessien polygons to divide the cluster area of NTL. It is convenient and easy to understand, but it needs to optimize the division method of urban agglomeration area further. For example, traffic accessibility [68], the level of industry complementary [69], and other factors need to be considered as the possible division basis at the fine-scale imagery rather than just using space distance and NTL data herein. NTL was proved to be an explanatory covariant for the macrospatial pattern with the capability to delineate human activity. Moreover, the verification of urban subregions (i.e., urban core area, urban–rural fringe, and rural area) is still a difficult problem nevertheless the method of qualitative analysis using EVI has been proposed [31]. Therefore, visual verification based on Google high-resolution images is adopted. Third, our results revealed that NTL has the most prominent interaction with GSD or with ASD, which was responsible for explaining more than 90% of the spatial variation of the SUHI pattern. Therefore, NTL is likely to be the new proxy or the new driving factor that need be taken into account in other two SUHII measuring methods. Furthermore, exploring the possible relation of NTL with LST pattern or simulation with the impact factors can be carried in the future study.

VI. CONCLUSION

With the rapid development of the urban agglomeration, which continues to pose challenges for the urban environment of human being, this article presents an integrated analysis framework for spatial pattern of SUHI in urban agglomerations. We incorporated the capacity of NTL for human footprint into the multicenters pattern analysis of urban agglomeration. It is crucial that proposing a new method for RLST selection in the NTL_Thessien polygons to delineate the various complex thermal environments accurately and adaptively. The experimental results for the SUHII estimation by using the RLST of suburban, forest, and the proposed rural areas demonstrated that multicenters and NTL_Thessien polygons were the important units. The proposed mcSUHII method is helpful to mitigate the underestimation bias of SUHII as well as to indicate the microclimate pattern in inland and coastal areas in GHMBay. The results of the study proved that the change in SUHII for urban agglomerations is greater than for a single city based on the case of GHMBay. The use of Geodetector further illustrated that the interaction of NTL and ASD, ESD was dominated the inland and the whole thermal environment in GHMBay. The article demonstrated the estimation of SUHII in multicenters of urban agglomeration from a new perspective of human activity on the thermal environment, which would provide suggestions supporting for the urban managers.

ACKNOWLEDGMENT

The authors would like to thank the anonymous reviewers for helping improve this manuscript.

REFERENCES

[1] L. Howard, "Climate of London deduced from metrological observations," *Harvey Dolton*, vol. 1, no. 2, pp. 1–24, 1833.
[2] T. R. Oke, "City size and the urban heat island," *Atmos. Environ.*, vol. 7, no. 8, pp. 769–779, 1973.
[3] S. Peng *et al.*, "Surface urban heat island across 419 global big cities," *Environ. Sci. Technol.*, vol. 46, no. 2, pp. 696–703, 2012.

[4] P. Vahmani and G. A. Ban-Weiss, "Impact of remotely sensed albedo and vegetation fraction on simulation of urban climate in WRF-urban canopy model: A case study of the urban heat island in Los Angeles," *J. Geophys. Res.-Atmos.*, vol. 121, no. 4, pp. 1511–1531, 2016.

[5] F. Chen *et al.*, "The integrated WRF/urban modelling system: Development, evaluation, and applications to urban environmental problems," *Int. J. Climatol.*, vol. 31, no. 2, pp. 273–288, 2011.

[6] J. A. Voogt and T. R. Oke, "Thermal remote sensing of urban climates," *Remote Sens. Environ.*, vol. 86, no. 3, pp. 370–384, 2003.

[7] P. K. Rao, "Remote sensing of urban" heat islands" from an environmental satellite," *Bull. Amer. Meteorol. Soc.*, vol. 53, no. 7, pp. 647–648, 1972.

[8] D. Zhou *et al.*, "Satellite remote sensing of surface urban heat islands: Progress, challenges, and perspectives," *Remote Sens.*, vol. 11, no. 1, pp. 1–36, 2019.

[9] K. Deilami, M. Kamruzzaman, and Y. Liu, "Urban heat island effect: A systematic review of spatio-temporal factors, data, methods, and mitigation measures," *Int. J. Appl. Earth Observ. Geoinf.*, vol. 67, pp. 30–42, 2018.

[10] R. Anniballe, S. Bonafoni, and M. Pichierri, "Spatial and temporal trends of the surface and air heat island over Milan using MODIS data," *Remote Sens. Environ.*, vol. 150, pp. 163–171, 2014.

[11] U. Rajasekar and Q. Weng, "Urban heat island monitoring and analysis using a non-parametric model: A case study of Indianapolis," *Int. Soc. Photogrammetry Remote Sens.*, vol. 64, no. 1, pp. 86–96, 2009.

[12] N. Schwarz, S. Lautenbach, and R. Seppelt, "Exploring indicators for quantifying surface urban heat islands of European cities with MODIS land surface temperatures," *Remote Sens. Environ.*, vol. 115, no. 12, pp. 3175–3186, 2011.

[13] J. Lai *et al.*, "Identification of typical diurnal patterns for clear-sky climatology of surface urban heat islands," *Remote Sens. Environ.*, vol. 217, pp. 203–220, 2018.

[14] Q. Weng, D. Lu, and J. Schubring, "Estimation of land surface temperature–vegetation abundance relationship for urban heat island studies," *Remote Sens. Environ.*, vol. 89, no. 4, pp. 467–483, 2004.

[15] D. Zhou, D. Li, G. Sun, L. Zhang, Y. Liu, and L. Hao, "Contrasting effects of urbanization and agriculture on surface temperature in eastern China," *J. Geophys. Res.-Atmos.*, vol. 121, no. 16, pp. 9597–9606, 2016.

[16] X. Chen, H. Zhao, P. Li, and Z. Yin, "Remote sensing image-based analysis of the relationship between urban heat island and land use/cover changes," *Remote Sens. Environ.*, vol. 104, no. 2, pp. 133–146, 2006.

[17] S. Haashemi, Q. Weng, A. Darvishi, and S. Alavipanah, "Seasonal variations of the surface urban heat island in a semi-arid city," *Remote Sens.*, vol. 8, no. 4, pp. 1–17, 2016.

[18] Y. Liu, X. Fang, Y. Xu, S. Zhang, and Q. Luan, "Assessment of surface urban heat island across China's three main urban agglomerations," *Theor. Appl. Climatol.*, vol. 133, pp. 473–488, 2017.

[19] J. Quan, W. Zhan, Y. Chen, M. Wang, and J. Wang, "Time series decomposition of remotely sensed land surface temperature and investigation of trends and seasonal variations in surface urban heat islands," *J. Geophys. Res. Atmos.*, vol. 121, no. 6, pp. 2638–2657, 2016.

[20] D. Zhou, S. Bonafoni, L. Zhang, and R. Wang, "Remote sensing of the urban heat island effect in a highly populated urban agglomeration area in East China," *Sci. Total Environ.*, vol. 628/629, pp. 415–429, 2018.

[21] J. Wu, "Urban ecology and sustainability: The state-of-the-science and future directions," *Landscape Urban Planning*, vol. 125, pp. 209–221, 2014.

[22] C. Fang and D. Yu, "Urban agglomeration: An evolving concept of an emerging phenomenon," *Landscape Urban Planning*, vol. 162, pp. 126–136, 2017.

[23] D. Zhou, L. Zhang, L. Hao, G. Sun, Y. Liu, and C. Zhu, "Spatiotemporal trends of urban heat island effect along the urban development intensity gradient in China," *Sci. Total Environ.*, vol. 544, pp. 617–626, 2016.

[24] H. Du *et al.*, "Influences of land cover types, meteorological conditions, anthropogenic heat and urban area on surface urban heat island in the Yangtze river delta urban agglomeration," *Sci. Total Environ.*, vol. 571, pp. 461–470, 2016.

[25] Z. Xue *et al.*, "Quantifying the cooling-effects of urban and peri-urban wetlands using remote sensing data: Case study of cities of Northeast China," *Landscape Urban Planning*, vol. 182, pp. 92–100, 2019.

[26] P. Berdahl and S. E. Bretz, "Preliminary survey of the solar reflectance of cool roofing materials," *Energy Buildings*, vol. 25, no. 2, pp. 149–158, 1997.

[27] L. Hu and J. Wendel, "Analysis of urban surface morphologic effects on diurnal thermal directional anisotropy," *Int. Soc. Photogrammetry Remote Sens.*, vol. 148, pp. 1–12, 2019.

[28] J. Hofierka, M. Gallay, K. Onačillová, and J. Hofierka, "Physically-based land surface temperature modeling in urban areas using a 3-D city model and multispectral satellite data," *Urban Climate*, vol. 31, 2020, Art. no. 100566.

[29] D. Lu, S. Hetrick, and E. Moran, "Land cover classification in a complex urban-rural landscape with QuickBird imagery," *Photogrammetric Eng. Remote Sens.*, vol. 76, no. 10, pp. 1159–1168, 2010.

[30] R. TV, B. H. Aithal, and D. D. Sanna, "Insights to urban dynamics through landscape spatial pattern analysis," *Int. J. Appl. Earth Observ.*, vol. 18, pp. 329–343, 2012.

[31] J. Peng, Y. Liu, J. Ma, and S. Zhao, "A new approach for urban-rural fringe identification: Integrating impervious surface area and spatial continuous wavelet transform," *Landscape Urban Planning*, vol. 175, pp. 72–79, 2018.

[32] J. Peng, P. Xie, Y. Liu, and J. Ma, "Urban thermal environment dynamics and associated landscape pattern factors: A case study in the Beijing metropolitan region," *Remote Sens. Environ.*, vol. 173, pp. 145–155, 2016.

[33] Y. Fu, X. Lu, Y. Zhao, X. Zeng, and L. Xia, "Assessment impacts of weather and land use/land cover (LULC) change on urban vegetation net primary productivity (NPP): A case study in Guangzhou, China," *Remote Sens.*, vol. 5, no. 8, pp. 4125–4144, 2013.

[34] Z. Zhu *et al.*, "Including land cover change in analysis of greenness trends using all available Landsat 5, 7, and 8 images: A case study from Guangzhou, China (2000–2014)," *Remote Sens. Environ.*, vol. 185, pp. 243–257, 2016.

[35] S. Zhao, S. Liu, and D. Zhou, "Prevalent vegetation growth enhancement in urban environment," *Proc. Nat. Acad. Sci. USA*, vol. 113, no. 22, pp. 6313–6318, 2016.

[36] Y. Dong, A. C. G. Varquez, and M. Kanda, "Global anthropogenic heat flux database with high spatial resolution," *Atmos. Environ.*, vol. 150, pp. 276–294, 2017.

[37] Z. Zhang, A. Zhang, and H. Guo, "Spatial recognition of the urban-rural fringe based on DMSP/OLS nighttime light data: A case study of the main urban areas of Chongqing," *Geography Geo-Inf. Sci.*, vol. 32, no. 6, pp. 37–42, 2016.

[38] S. Mustak, N. K. Baghmar, P. K. Srivastava, S. K. Singh, and R. Binolakar, "Delineation and classification of rural–urban fringe using geospatial technique and onboard DMSP—Operational linescan system," *Geocarto Int.*, vol. 33, no. 4, pp. 375–396, 2018.

[39] Y. Zhang and J. Cheng, "Spatio-temporal analysis of urban heat island using multisource remote sensing data: A case study in Hangzhou, China," *IEEE J. Sel. Top. Appl. Earth Observ. Remote Sens.*, vol. 12, no. 9, pp. 3317–3326, Sep. 2019.

[40] C. D. Elvidge, K. E. Baugh, E. A. Kihn, H. W. Kroehl, E. R. Davis, and C. W. Davis, "Relation between satellite observed visible-near infrared emissions, population, economic activity and electric power consumption," *Int. J. Remote Sens.*, vol. 18, no. 6, pp. 1373–1379, 1997.

[41] Z. Chen, B. Yu, Y. Hu, C. Huang, K. Shi, and J. Wu, "Estimating house vacancy rate in metropolitan areas using NPP-VIIRS nighttime light composite data," *IEEE J. Sel. Top. Appl. Earth Observ. Remote Sens.*, vol. 8, no. 5, pp. 2188–2197, May 2015.

[42] H. Taubenböck *et al.*, "A new ranking of the world's largest cities—Do administrative units obscure morphological realities?" *Remote Sens. Environ.*, vol. 232, 2019, Art. no. 111353.

[43] F. Peng, "Economic spatial connection and spatial structure of Dawan district and its surrounding cities in Guangdong, Hong Kong and Macao—An empirical analysis based on improved gravity model and social network analysis," *Econ. Geography*, vol. 37, no. 12, pp. 57–64, 2017.

[44] C. D. Elvidge *et al.*, "A fifteen year record of global natural gas flaring derived from satellite data," *Energies*, vol. 2, no. 3, pp. 595–622, 2009.

[45] Z. Cao, Z. Wu, Y. Kuang, and N. Huang, "Correction of DMSP/OLS night-time light images and its application in China," *J. Geo-Inf. Sci.*, vol. 17, no. 9, pp. 1092–1102, 2015.

[46] Z. Chen *et al.*, "A new approach for detecting urban centers and their spatial structure with nighttime light remote sensing," *IEEE Trans. Geosci. Remote Sens.*, vol. 55, no. 11, pp. 6305–6319, Nov. 2017.

[47] M. J. McCullagh and C. G. Ross, "Delaunay triangulation of a random data set for isarithmic mapping," *Cartographic J.*, vol. 17, no. 2, pp. 93–99, 1980.

[48] K. E. Brassel and D. Reif, "A procedure to generate Thiessen polygons," *Geographical Anal.*, vol. 11, no. 3, pp. 289–303, 1979.

[49] J. Peng *et al.*, "Spatial-temporal change of land surface temperature across 285 cities in China: An urban-rural contrast perspective," *Sci. Total Environ.*, vol. 635, pp. 487–497, 2018.

[50] Y. Yang, M. Ma, C. Tan, and W. Li, "Spatial recognition of the urban-rural fringe of Beijing using DMSP/OLS nighttime light data," *Remote Sens.*, vol. 9, no. 11, 2017, Art. no. 1141.
[51] H. Fan, W. Liu, and Z. Wu, "Spatio-temperal characteristics of internal coordination of intensive urban land use: A case study of the downtown of Wuhan," *Scientia Geographica Sinica*, vol. 34, no. 6, pp. 696–704, 2014.
[52] W. Zhang, Y. Zhou, and G. Hu, "Coupling mechanism and space-time coordination of new-approach urbanization, new-approach industrialization and service industry modernization in megacity behemoths: A case study of ten cities in China," *Scientia Geographica Sinica*, vol. 33, no. 5, pp. 562–569, 2013.
[53] M. L. Imhoff, P. Zhang, R. E. Wolfe, and L. Bounoua, "Remote sensing of the urban heat island effect across biomes in the continental USA," *Remote Sens. Environ.*, vol. 114, no. 3, pp. 504–513, 2010.
[54] R. Sun, Y. H. Lü, L. Chen, L. Yang, and A. Chen, "Assessing the stability of annual temperatures for different urban functional zones," *Building Environ.*, vol. 65, pp. 90–98, 2013.
[55] A. Trlica, L. R. Hutyra, C. L. Schaaf, A. Erb, and J. A. Wang, "Albedo, land cover, and daytime surface temperature variation across an urbanized landscape," *Earth Future*, vol. 5, no. 11, pp. 1084–1101, 2017.
[56] K. Kourtidis *et al.*, "A study of the hourly variability of the urban heat island effect in the greater Athens area during summer," *Sci. Total Environ.*, vol. 517, pp. 162–177, 2015.
[57] N. Zhang, Y. Chen, L. Luo, and Y. Wang, "Effectiveness of different urban heat island mitigation methods and their regional impacts," *J. Hydrometeorology*, vol. 18, pp. 2991–3012, 2017.
[58] C. Hutengs and M. Vohland, "Downscaling land surface temperatures at regional scales with random forest regression," *Remote Sens. Environ.*, vol. 178, pp. 127–141, 2016.
[59] L. Gao *et al.*, "Disaggregation of remotely sensed land surface temperature: A simple yet flexible index (SIFI) to assess method performances," *Remote Sens. Environ.*, vol. 200, pp. 206–219, 2017.
[60] L. W. Siu and M. A. Hart, "Quantifying urban heat island intensity in Hong Kong SAR, China," *Environ. Monit. Assessment*, vol. 185, no. 5, pp. 4383–4398, 2013.
[61] Y. Yuan, C. Xi, Q. Jing, and N. Felix, "Seasonal variations of the urban thermal environment effect in a tropical coastal city," *Adv. Meteorol.*, vol. 2017, pp. 1–18, 2017.
[62] J. Wang *et al.*, "Geographical detectors-based health risk assessment and its application in the neural tube defects study of the Heshun region, China," *Int. J. Geographical Inf. Sci.*, vol. 24, no. 1, pp. 107–127, 2010.
[63] J. Wang and Y. Hu, "Environmental health risk detection with geodetector," *Environ. Model. Softw.*, vol. 33, pp. 114–115, 2012.
[64] W. Luo, J. Jasiewicz, T. Stepinski, J. Wang, C. Xu, and X. Cang, "Spatial association between dissection density and environmental factors over the entire conterminous united states," *Geophys. Res. Lett.*, vol. 43, no. 2, pp. 692–700, 2016.
[65] J. Wang and C. Xu, "Geodetector: Principle and prospective," *Acta Geographica Sinica*, vol. 72, no. 1, pp. 116–134, 2017.
[66] X. Li, X. Li, D. Li, X. He, and M. Jendryke, "A preliminary investigation of Luojia-1 night-time light imagery," *Remote Sens. Lett.*, vol. 10, no. 6, pp. 526–535, 2019.
[67] G. Zhang, J. Wang, Y. Jiang, P. Zhou, Y. Zhao, and Y. Xu, "On-orbit geometric calibration and validation of Luojia 1-01 night-light satellite," *Remote Sens.*, vol. 11, no. 3, pp. 1–19, 2019.
[68] M. J. Widener, S. Farber, T. Neutens, and M Horner, "Spatiotemporal accessibility to supermarkets using public transit: An interaction potential approach in Cincinnati, Ohio," *J. Transp. Geography*, vol. 42, pp. 72–83, 2015.
[69] K. Martinus and T. J. Sigler, "Global city clusters: Theorizing spatial and non-spatial proximity in inter-urban firm networks," *Regional Stud.*, vol. 52, no. 8, pp. 1041–1052, 2018.

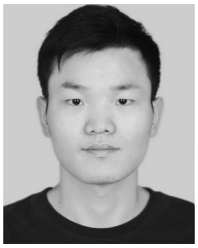

Jiufeng Li received the bachelor's degree from Guangzhou University, Guangzhou, China, in 2016, and the master's degree in GIS from South China Normal University, Guangzhou, China, in 2019. He is currently working toward the Ph.D. degree with Nanjing University, Nanjing, China.

His major research interest focuses on urban ecology based on remote sensing, mostly urban heat island effects.

Fangfang Wang received the bachelor's degree in GIS from the Henan University of Economics and Law, Zhengzhou, China, in 2016, and the master's degree in GIS from South China Normal University, Guangzhou, China, in 2019. She is currently working toward the Ph.D. degree with the Institute of Tibetan Plateau Research, Chinese Academy of Sciences, Beijing, China.

Her major research interests include atmospheric physics and atmospheric environment based on remote sensing.

Yingchun Fu received the B.S. degree in surveying and mapping engineering from the Technology and Science of Kunming University, Kunming, China, in 1997, and the Ph.D. degree in photogrammetry and remote sensing from Wuhan University, Wuhan, China, in 2006.

She is currently a Professor with the Geographical Information Science Division, South China Normal University, South China Normal University. From 2014 to 2015, she was a Visiting Scholar with the Earth And Environment Science Division, Boston University, Boston, MA, USA. She has authored/coauthored more than 30 research papers. Her research interests include high-resolution and time series remote sensing, change and detection, and geosimulation.

Prof. Fu was the recipient of the 2017 Highly Cited Paper Award from the *Journal of Geographical Science*. She serves as the reviewer for the *Journals of Remote Sensing*, *Science of the Total Environment*, and IEEE JOURNAL OF SELECTED TOPICS IN EARTH OBSERVATIONS AND APPLIED REMOTE SENSING.

Biyun Guo received the bachelor's degree in geographical information science from Hengyang Normal University, Hengyang, China, in 2018. She is currently working toward the master's degree with South China Normal University, Guangzhou, China.

Her major research interests include nighttime light remote sensing and its application in urban research.

Yaolong Zhao received the Ph.D. degree in geography from the University of Tsukuba, Tsukuba, Japan, in 2007.

He is currently a Professor of geographical information science with the South China Normal University, Guangzhou, China.

Huafei Yu received the bachelor's degree from Guangzhou University, Guangzhou, China, in 2016, and the master's degree in GIS from the South China Normal University, Guangzhou, China, in 2019. He is currently working toward the Ph.D. degree with Wuhan University, Wuhan, China.

His research interests include geographic simulation and deep learning in map space.